Title
LOW-HEAT-LEAK CURRENT LEADS FOR INTERMITTENT USE

Authors
Smoot, G.F.
Pope, W.L.

Publication Date
1974-04-01

LBL-2690
Preprint

Submitted to Advances in
Cryogenic Engineering

LOW-HEAT-LEAK CURRENT LEADS FOR INTERMITTENT USE

G. F. Smoot and W. L. Pope

April 1974

Prepared for the U.S. Atomic Energy Commission
under Contract W-7405-ENG-48

DISCLAIMER

LBL-2690

LOW-HEAT-LEAK CURRENT LEADS FOR INTERMITTENT USE*

G. F. Smoot and W. L. Pope

Space Sciences Laboratory
and Lawrence Berkeley Laboratory**

University of California, Berkeley
Berkeley, California

April 1974

ABSTRACT

Many cryogenic systems have current leads operating with a short duty cycle. An example of this is a superconducting magnet which is used in a persistent current mode for long periods, the current leads being used only for short periods for charging or discharging the superconducting magnet. A more economical design operates the current leads close to thermal instability in order to minimize the dominant long term heat leak at zero current. When system considerations dictate the use of insulated leads, low-heat-leak design is particularly challenging. We have designed and tested a pair of tapered, composite, gas-cooled, insulated leads for this mode of operation. A relatively simple computer program accurately fits the test results, including predictions of the instability current.

---

* This work supported by NASA contracts NAS 8-27408 and NAS 8-7801.

** An AEC-supported Laboratory.

INTRODUCTION

Cryogenic systems with short duty cycles use less liquid helium if their current leads are operated at more than their optimum current. We have designed and tested insulated gas-cooled leads whose zero current heat leak is about five times less than a perfectly insulated lead [1] and is 40% less [2,3] than an optimal uninsulated lead for the same operating current.

Previous authors [2-4] have described gas-cooled, uninsulated, cryogenic current leads capable of carrying currents up to 10,000 amperes. In most of these systems, the leads were designed to carry current continuously, and were optimized to produce the lowest total heat leak at the design current. These optimization techniques are now generally accepted and computer programs have been written [5] which satisfactorily predict lead performance for simple configurations.

Our cryogenic system is an orbiting superconducting magnetic spectrometer [6; see preceding paper] intended to operate in space for one year. The satellite weight budget restricts us to only about 430 kg of liquid helium, so we can tolerate a total heat leak of no more than a quarter watt. Obviously the steady state heat leak for lead conduction must be limited to about 1/10 watt. For reliability the spectrometer design requires two redundant insulated lead pairs, each capable of carrying 120 amperes and each pair restricted to a zero current heat leak of 0.05 watt.

Such a low heat leak has not been achieved [5] even with uninsulated optimum charge leads, so we were forced to investigate alterations such as tapering the leads, adding superconducting sections, and operating above the optimum current.

Off-optimum, insulated, tapered, composite leads have not been covered

in the literature, so we developed the required analysis tools.

CRYOSTAT-MAGNET SYSTEM DESIGN

Figure 1 is a schematic drawing of the cryostat currently being fabricated by the AiResearch Division of Garrett. The insulated magnet charging leads are contained in the cryostat fill-vent line. During the approximately four hours of magnet charging, an externally powered heater maintains the helium gas flow necessary to cool the current leads. Once the magnet is charged, the heater power is interrupted and the reduced gas flow cools only the innermost end (1.55 meters) of the leads and then diverts to the steady-state-vent which coils about the vapor-cooled shields of the cryostat.

During the short charging period a relatively high flow rate (0.7 g/sec) allows the leads to operate well above their optimal current and thus be physically small for the subsequent long zero-current steady state.

PHENOMENOLOGICAL BEHAVIOR

For cryogenic current leads of constant cross section constructed of relatively pure metals like copper, whose resistivity increases with increasing temperature, thermal instability occurs at or near the hot end of the lead. The zero current heat leak is higher than absolutely necessary, since it can be reduced by tapering the leads with no loss in current capacity. [7] If the lead cross section varies too abruptly, thermal instability will occur closer to the cold end of the lead. At temperatures $\lesssim 50°K$ and high current, thermal instability occurs very rapidly because the resistivity increases approximately as T^4 and because of the lead's reduced heat capacity. This cold end instability can occur on all insulated tapered leads operating at higher than the optimum current. The instability boundary can be predicted with suitable modeling.

ANALYSIS

Consider (as shown in Fig. 2) an element of a long insulated current lead in thermal contact with cryogenic gas flow.

If we define q as the net heat accumulating in the element per unit length per unit time, then

$$q\,dx = dQ_A - q_L dx + q_V dx .$$

Divide through by dx and this expression becomes.

$$q = \frac{dQ_A}{dx} - q_L + q_V$$

$$= \frac{d}{dx}\left(kA\frac{dT}{dx}\right) - \frac{1}{R_T}(T - T_{gas}) + \frac{\rho I^2}{A}$$

In steady state the net heat flow per unit length, q, into the element must be zero or it will heat up or cool down due to its finite heat capacity. This thermal equilibrium (balance between heating and cooling) will be stable if $dq/dT < 0$, so that if the temperature of the element increases, heat will flow out and the element will cool, or if the temperature decreases, heat will flow into the element and warm it.

> Criteria for a Stable Steady State:
>
> (a) equilibrium: $q = 0$,
>
> (b) stability: $\frac{dq}{dT} < 0$,
>
> where T = temperature and
>
> q = heat per unit length into lead.

In most cases the only significant heat flow into the gas is from the wire so that

$$q_L = C_P \frac{dm}{dt}\frac{dT_{gas}}{dx} = C_P \dot{m}\frac{dT_{gas}}{dx}$$

where C_P is the specific heat of the gas and $\dot{m}$ is the mass flow. This formula integrates to

$$T_{gas} = T_o + \int_o^x \frac{q_L}{C_P \dot{m}}\, dx$$

$$= T_o + \int_o^x (T - T_{gas}) / \left(R_T C_P \dot{m}\right) dx.$$

Thus if we have expressions for the electrical resistivity, ρ, the thermal resistance per unit length, R_T, of the insulation and gas film and the thermal conductivity, k, of the conductor, we can find the steady state temperature distribution for the current lead by setting $q = 0$ and solving the resulting equation.

Electrical Resistivity - ρ

Mattiessen's rule states that the electrical resistivity of a metal may usually be written in the form [8]

$$\rho = \rho_o + \rho_T(T)$$

where the residual resistivity, ρ_o, is independent of temperature and depends on the concentration of impurity atoms and mechanical imperfections of the sample; while $\rho_T(0) = 0$ and $\rho_T(T)$ is characteristic of the metal.

Grüneisen [8] has found that the observed temperature dependence of the resistivity is described quite well at all temperatures by the semi-empirical formula

$$\rho_T(T) \propto \left(\frac{T}{\theta}\right)^5 \int_0^{\theta/T} \frac{x^5 e^x dx}{(e^x - 1)^2}$$

where θ is a characteristic temperature near the Debye temperature of the metal. For copper we have used $\theta = 333\,^{\circ}K$ and $\rho_T(\theta) = 2.1 \times 10^{-6}\,\Omega$-cm. Figure

3 is a plot of the resulting theoretical resistivity of copper. Note that, as suggested by J. M. Lock [9], $\rho = \rho_o + 8.7 \cdot 10^{-15} T^4$ is in good agreement with this theory and the data below 50°K, especially since below about 25°K the residual resistivity of the copper masks the temperature dependence. Appendix A is a listing of the computer program we use to evaluate $\rho_T(T)$.

Thermal Resistance Per Unit Length - R_T

The thermal resistance per unit length, R_T, is the sum of the resistance due to the insulation and due to the gas film. The insulation thermal resistance per unit length is just

$$R_i = \frac{t_i}{C_{im}} \frac{1}{k_i}$$

where t_i is the insulation thickness, C_{im} is the mean insulation circumference, and k_i is the thermal conductivity of the insulation. We did not know the insulation conductivities, so we estimated them from heat balance consideration of early tests. Although the calculated insulation conductivities are the same order as other plastics for these temperatures ($k_i \approx 2.5 \times 10^{-4}$ watts/cm-°K) we do not know how accurate they are. Typically the insulation resistance is about half the total thermal impedance for our final lead design.

We calculated the resistance due to the gas film using the formula for a heated rod in a tube with turbulent flow:

$$R_{gas} = \frac{D_e}{C_o} \frac{1}{k_{He} \times Nu} ,$$

where

D_e = effective heat transfer diameter of the tube,

C_o = outer perimeter of the insulation in contact with the gas,

k_{He} = helium gas thermal conductivity $\approx 2.4\times10^{-5}\,(T_{He})^{0.73}$ watts/cm-°K,

Nu = Nusselt number $= 0.02\times Re^{0.8}\times Pr^{0.333}\left(\frac{D_{tube}}{D_{insulation}}\right)^{0.53}$ [10]

Re = Reynolds number, Pr = Prandtle number,

ν_{He} = the viscosity of the gas $= 5.023\times10^{-6}\,(T_{He})^{0.647}$ [11].

The net result is that the thermal impedance of the gas is approximately proportional to $T^{-0.2}\,\dot{m}^{-0.8}$.

Thermal Conductivity - k

At low temperatures most metals obey the Wiedmann-Franz law $k\rho_o = L_o T$, where $L_o = 1/3\pi^2\left(\frac{k_B}{e}\right)^2 = 2.445\times10^{-8}$ watt-Ω-cm/°K and ρ_o is the residual resistivity. Furthermore the temperature variation of $k\rho/T = L(T)$ = Lorenz number is relatively small (about a factor of 2) and known [9]. The thermal conductivity of copper is typically 10 watts/cm-°K for our case.

Calculation of Lead Performance

With these expressions we can then calculate, using numerical techniques, the steady state temperature profile and other parameters for a lead carrying current. For example, we could use either the Runge-Kutta method as suggested by N. Inai [12] or the boundary values and the method of finite differences.

However, in the case of our charge leads we note two conditions: (1) The characteristic distance $\lambda = \sqrt{kA\cdot R_T}$ over which thermal conduction is important is typically about 2 to 5 cm. Our lead sections are on the order of 100 cm; therefore, lateral conduction dominates axial conduction for reasonable mass flows. (2) We have finned-tube heat exchangers at the warm end of the leads. For reasonable current and gas flows the ohmic heating and gas cooling in the finned tubes dominates conduction from the electrical and mech-

anical contacts, thereby effectively thermally divorcing the leads from the outside world. We can neglect axial conduction except very near the lead section joints and our heat balance equation simplifies to

$$q = \frac{\rho I^2}{A} - \frac{1}{R_T}(T - T_{gas}), \quad \text{which is zero in steady state.}$$

Thus, the temperature of the wire is

$$T = T_{gas} + R_T \frac{\rho I^2}{A}$$

which is a nonlinear equation in T and can be solved simply by iteration. The heat balance is illustrated graphically in Fig. 4 for an arbitrary location along the lead.

Lead Test Apparatus

The leads were tested in a 362 cm long vacuum-insulated section of 0.95 cm outer diameter by 0.041 mm wall stainless steel tube which simulates the physical size of the fill-vent line of the thermal model cryostat [6]. Four leads were contained in the tube -- two leads were used to carry the test current and two were used as heater leads. For the tests the vacuum-insulated lead tube was inserted into the neck of a standard 50 liter, liquid-nitrogen-cooled, liquid helium dewar. The two current leads were simply soldered together and the cold end was kept immersed in liquid helium. The two heater leads were connected to a 14 watt carbon resistance heater (48 Ω at 4.2°K), also kept in the liquid helium.

Figure 5 is a schematic drawing of the test setup. The total length of all leads between point A and B is 362 cm. Below point A, the superconducting portion of the current leads continued to the bottom of the dewar with a 60 cm length of #16 AWG Mylar tape insulated annealed solid copper wire soldered

in parallel to minimize any temperature rise and heat disipation in that portion which is above the liquid level but not cooled by forced convection.

Above point B in Fig. 5 each of the four leads were terminated with a 3.3 mm diameter by 15 cm long current-carrying brass rod machined with 8.90 mm outer diameter by 0.5 mm thick external spiral fins with a pitch of 3.94 turns per cm. This finned brass rod, which we call a finned-tube heat exchanger was contained in a close-fitting 0.95 cm outer diameter by 0.025 mm thick stainless steel tube.

During testing, all of the helium vapor flow was routed up in the lead tube to just the two finned-tube heat exchangers which terminated the two high current leads.

This finned-tube heat exchanger was designed to suit requirements specified by Ball Brothers Research Corp. (Boulder, Colorado) as a result of their earlier computer analysis. Their studies showed that high-current stable operation could be achieved with off-optimum small-diameter insulated copper leads cooled by laminar flow in a tube if the hot ends were terminated with a short section (10 cm) of conductor with a significantly higher (factor of 10) surface cooling per unit length than the last section of lead.

Total pressure drop through the simulated vent line with two finned-tube heat exchangers in parallel at the end is 2.5 psi at 130 amp with a helium flow rate of 0.70 g/sec. This is of course turbulent flow; the significant influence of a small amount of insulation on the leads was previously greatly underestimated.

First Test Lead Configuration

Table I is a description of the first tapered lead configuration tested.

The residual resistivity of the top and middle wire sections was premeasured using 2.0 m long samples of wire in a standard 50 liter liquid helium dewar. The residual resistivity (Table I) of the copper matrix of the superconducting section is approximately correct. It was calculated from the abrupt incremental voltage changes measured across that section of the actual lead as it transitioned from the superconducting to the normal state under test, prior to complete thermal instability farther up the lead.

Voltage taps were placed on the two current leads at the joints and at either end of the finned-tube heat exchangers. The voltage sense leads were #30 AWG Teflon-insulated copper wire that exited the vent tube region through a glass-sealed header in the charge lead bayonet. Voltages were monitored on a digital volt meter and two strip chart recorders.

Figure 6 is a plot of lead voltage drop versus current for tests conducted on the first lead configuration (Table I). These data were taken for various helium flow rates between 0.03 g/sec and 0.97 g/sec. The linear current voltage solid lines are a good indication that the lead temperature distribution (resistance) does not change substantially with flow rate and also current if the lower section is superconducting.

Two distinctly different operating modes can be noted from Fig. 6: (1) the solid line when the superconducting lower lead segment is maintained below about 10°K and is, therefore, non-resistive, and (2) when the lower lead section is above the transition temperature of Nb-Ti.

Either operating mode could be attained at will. If the initially established helium mass flow was maintained at a high rate above currents of about 25 to 30 amps, the lower voltage trajectory (solid lines) was followed up until about 100 to 110 amps, when the superconductor transitioned. About two seconds later, the strip chart recorder voltage data showed that the temperature of

the middle section of #20 gage wire started to rise as complete thermal runaway set in.

Conversely, if the helium flow rate was initially low, with a resistive superconducting composite segment, the higher voltage trajectory (dashed lines) was followed from about 25 to 30 amps until the lead became thermally unstable.

Figure 7 is a plot of helium coolant mass flow rate versus current for the first lead configuration tested. The solid curve was plotted from computer program output data using our stability criteria.

Final Lead Configuration

The first lead configuration could not meet the minimum acceptable design current of 120 amps. An analysis of the data and sensitivity studies with the computer program indicated that the following three relatively minor lead changes would suffice.

(1) Reduce the insulation thickness on the lower and middle lead segments. Use two spiral wraps of 0.025 mm thick Mylar tape (max).

(2) Obtain lower residual resistivity #20 AWG copper wire for the middle lead segment. Sample testing was required.

(3) Increase the lower leg superconducting part from 0.762 mm diameter 1.8/1.0 Cu-SC ratio Nb-Ti wire to 0.812 mm diameter wire of the same type.

The new wire was on hand, purchased from the same vendor, but the cladding residual resistivity was unknown. It was assumed to be the same as the old wire. We measured the residual resistivity on twelve 2.0 m long copper wire samples. A sample of Formvar insulated #20 AWG solid annealed copper wire (LBL magnet wire) was found to have a residual resistivity of 8.1×10^{-9}

Ω-cm, which would be acceptable, but this increased 250% with as little as 15% permanent strain. It was very difficult to hand-wrap without some cold working, so a special Mylar tape-wrapping device was rigged on an engine lathe. After a two-layer spiral wrap of tape was applied to the Magnet wire, no change in residual resistivity could be detected. Table II lists the details of the final lead configuration. The final lead configuration was given three separate current tests:

(1) current up to 125 amps at $\dot{m} \cong 0.7$ g/sec (3 times),

(2) current up to 135 amps at $\dot{m} \cong 0.7$ g/sec at 5 amp/min,

(3) current up to 80 amps at $\dot{m} \cong 0.35$ g/sec.

The lower section of lead was kept in the superconducting state for the above three tests. We took the lead to thermal instability two times at 129 and 127.5 amps in (1) above, which indicated the lead was not excessively over-designed. Figure 8 shows typical lead resistive heating versus length behavior for seven test currents up to 131 amps and four arbitrarily selected calculated conditions. Very good agreement with the data can be noted. The final lead design meets the 120 ampere design objective if maintained with the lower section superconducting, and this mode of operation is adequately modeled. With the lower section resistive we predict the lead will carry a maximum current of about 135 amps with a mass flow of 0.70 g/sec. The final lead configuration is clearly not optimized, it simply satisfies the 120 ampere requirement in a predictable fashion and has a sufficiently low steady state heat leak. The voltage drop per lead is about 50 mV at the design current, not including voltage drop through the finned-tube heat exchanger.

Steady State Tests

After the current tests were concluded the lead-vent simulation apparatus was used to determine the steady state (zero current) heat leak for the four

charge leads when only the lower 1.5 m were cooled. This test was conducted in two parts. First we measured the total flow rate out of the dewar resulting from: (1) zero current heat leak of the leads and lead vent, (2) parasitic heat into the dewar, and (3) heat generated in the liquid helium from the calibrated heater resistor. This total flow rate is shown in Fig. 9. We then removed the lead-vent simulator and measured the total flow rate out of the same dewar for various amounts of heat generated in the liquid helium by another calibrated high resistance heater which was attached at the bottom of a long 3.18 mm outside diameter by 0.152 mm thick stainless steel tube. The dewar heat leak was found to be 36 mW (1.07 SCF/H). Finally, with an iterative calculation procedure using our cryostat design program, we estimate the leads and lead vent will result in a net heat leak of 0.110 ± 0.01 watts (4 leads) into the Thermal Model Cryostat pressure vessel for the baseline design vapor expulsion mass flow rate of 0.011 g/sec (0.088 lb/hr).

This charge lead heat leak is about 42% of the baseline total system vapor expulsion heat leak of 0.26 watts. Although this is a large part of the total heat leak, the vapor-cooled shielded cryostat thermal protection system [6] (which has been optimized for liquid expulsion) has a relatively flat optimum for both vapor and liquid expulsion. Increasing the direct pressure vessel heat leak improves shield cooling, which in turn reduces the heat leak via the multilayer insulation and shield shorted supports with only a modest total heat leak increase. We find that if we were to eliminate the four charge leads and pressure vessel instrumentation leads associated with the magnet (10 each of #30 AWG copper wires), the total cryostat heat leak would only be reduced about 20% and 14% respectively for liquid and vapor expulsion. Therefore with the four charge leads connected as we have done in Fig. 1, we provide magnet protection and maintain acceptable overall system thermal performance.

CONCLUSIONS

Thermally efficient, insulated composite current leads can be designed for intermittent use. If the total system mass flow is used to cool the cold end of the leads and is subsequently used to reduce other parasitic heat into the system, the overall system thermal performance is only slightly affected by the presence of the leads.

Operating the insulated leads at well above their optimum current for short periods at high mass flow presents no insurmountable difficulties, and instability behavior is predictable.

ACKNOWLEDGMENTS

We thank E. Urban at Marshall Space Flight Center (Huntsville, Ala.); R. Herring and R. Poley at Ball Brothers Research Corp. (Boulder, Colo.); and T. Duffy at Lawrence Livermore Laboratory (Livermore, Calif.) for their contributions in preliminary design and analysis. We also thank J. Smithson at Johnson Space Center (Houston, Tex.) for arranging fabrication of much of the test apparatus.

In addition we express our appreciation to the following members of our group– H. Dougherty, J. Gibson and J. Yamada for their support and assistance in this project.

APPENDIX A

Computer Program for Evaluating $\rho(T)$

The following program computes the temperature-dependent component of the electrical resistivity, $\rho_T(T)$, for copper and other metals if the characteristic temperature, θ, (near the Debye temperature) and $\rho(\theta)$ is known.

The resistivity can then be calculated using Matthiessen's rule;

$$\rho = \rho_T(T) + \rho_o$$

where ρ_o is the residual resistivity.

The computer program equations match the semi-empirical Grüneisen theory to within:

0.1% for	$\theta/T > 6.0$,	low temperature regime;
0.3% for	$6.0 > \theta/T > 3.0$,	intermediate temperatures;
0.15% for	$3.0 > \theta/T$,	high temperature regime.

Details are contained in University of California, Space Sciences Laboratory Astrophysical Note No. 250 (2/20/74) available upon request.

```
      FUNCTION RHOT(T)
C     USE APPROXIMATION TO GRUNEISEN INTEGRAL FOR METAL RESTIVITY
C     PUT IN CHARACTERISTIC TEMPERATURE AND RESTIVITY FOR COPPER
      COMMON/RESIST/DRHODT
      DEBYE = 333.0
      RHOD = 2.1 E -06
C
      TD = T/DEBYE
      X = 1.0/TD
      E = EXP(X)
      SECOND = RHOD/0.23663/DEBYE*X*X*E/(E-1.0)**2
      If(X.GT.6.0)          GO TO 30
      IF(X.LT.3.0)          GO TO 10
C
C     CONNECT THE TWO TEMPERATURE DEPENDENCE REGIONS TOGETHER
C
      G = 50.275 + 21.343*(X - 5.0) - 0.648*(X-5.0)**3
      RHOT = TD**5*RHOD*G/0.23663
      DRHODT = 5.0*RHOT/T - SECOND
      RETURN
C
C     HIGH TEMPERATURE REGIME - RESISTIVITY PROPORTIONAL TO TEMPERATURE
C
   10 CONTINUE
      CAL = 0.25 - X**2/72.0 + X**4/1920.0 - X**6/60480.0
```

```
     1 + X**8/2073600.0 - X**10/74511360.0 + X**12/2752636480.0
      RHOT = TD*RHOD*CAL/0.23663
      DRHODT = 5.0*RHOT/T - SECOND
      RETURN
C
C     LOW TEMPERATURE REGIME - RESISTIVITY PROPORTIONAL TO T TO THE FIFTH
C
   30 CONTINUE
      GT = 124.431
      F = X**5 + 5.0*X**4 + 20.0*X**3 + 60.0*X**2 + 120.0*X + 120.
      G = GT - F*EXP(-X)
      RHOT = TD**5*RHOD*G/0.23663
      DRHODT = 5.0*RHOT/T - SECOND
      RETURN
      END
```

REFERENCES

1. R. McFee, Rev. Sci. Instrum. 30: 102 (1959).

2. P. Thullen, "A New Criterion for the Design of Gas-Cooled Cryogenic Current Leads," in: Advances in Cryogenic Engineering, Vol. 16, Plenum Press, New York (1971), p. 292.

3. J. M. Lock, Cryogenics 9 (6): 442 (1969).

4. V. E. Keilin and E. Yu. Klimenko, Cryogenics 6 (4): 222 (1966).

5. C. D. Henning, in: Proceedings of the Brookhaven National Laboratory Study on Superconducting Devices and Accelerators, Upton, New York (1968).

6. W. L. Pope et. al., "Superconducting Magnet and Cryostat for a Space Application," in: Advances in Cryogenic Engineering, Vol. 20, Plenum Press, New York (1974), p.

7. D. Eckert, M. Endig, and F. Lang, Cryogenics 10 (2): 138 (1970).

8. J. Bardeen, J. Appl. Phys. 11: 88 (1940).

9. J. M. Lock, Cryogenics 9 (6): 438 (1969).

10. M. Jacob, Heat Transfer, Vol. I, John Wiley & Sons, New York (1949), p. 552.

11. R. B. Scott, Cryogenic Engineering, D. Van Nostrand Co., New York (1959), p. 314

12. N. Inai, Cryogenics 9 (2): 115 (1969).

Table I. First Lead Configuration

Section	Top	Middle	Bottom
Material type (gage)	Insulated 19 strand ETP copper (#16 AWG)	Insulated 19 strand OFHC copper (#20 AWG)	Insulated** Nb-Ti, Cu clad 1.8/1 Cu-SC ratio
Diameter (mm)	1.291	0.812	0.608 (copper effective dia.)
Approx. length (cm)	132.	153.	77.
Measured residual resistivity, ρ_o(Ω-cm)	1.63×10^{-8}	1.44×10^{-8}	1.4×10^{-8}*
Insulation type	Kapton/FEP	Kapton	Kapton**
Insulation thickness (mm)	0.280	0.178	0.178

Joints in the leads are 2.0 inch long overlaps made with 50/50 Pb-Sn solder and wrapped with two layers of 0.002 inch thick Mylar tape.

*Calculated from test data voltage change when bottom section transitioned.

**Removed from the #20 AWG wire and slipped on the superconducting wire.

Table II. Final Lead Configuration Details

Lead Section	Top	Middle	Bottom
Material type (AWG)	19 strand ETP copper (#16)	Solid annealed magnet wire (#20)	Nb-Ti, Cu-clad 1.8/1 Cu-S.C. ratio
Diameter (mm)	1.291	0.812	0.651 (Cu effective diameter)
Approx. length (cm)	147.	153.	62.
Source	CFW*	LBL stock	MCA**
Measured residual resistivity, ρ_o(Ω-cm)	1.6×10^{-8}	0.81×10^{-8}	1.4×10^{-8} (assumed)
Insulated type	Kapton/FEP	Mylar tape‡	Mylar tape
Insulation thickness (mm)	0.280	$\approx$0.076‡	$\approx$0.051

‡Includes 0.025 mm of Formvar.

* California Fine Wire Corporation.

** Magnetic Corporation of America.

FIGURE CAPTIONS

Fig. 1. A schematic drawing of the cryostat. Note the plumbing and route of four charging current leads.

Fig. 2. Heat production and flow for an element of an insulated current lead.

$q_v dx$ = volume heat production = $\frac{\rho I^2}{A} dx$,

$q_L dx$ = lateral heat flow from the element = $\frac{1}{R_T} (T - T_{gas})\, dx$,

Q_A = axial heat flow = $kA \frac{dT}{dx}$;

where

T = lead temperature
I = lead current
ρ = lead resistivity
A = lead cross-sectional area
k = lead thermal conductivity
R_T = thermal resistance between lead and gas

Fig. 3. Resistivity of copper as a function of temperature. The solid curve (Grüneisen theory) was plotted using the computer program in Appendix A.

Fig. 4. Heat flow per unit length as a function of temperature. At T_1 there is stable equilibrium while at T_2 there is unstable equilibrium of heating and cooling. The gas temperature is found by integrating up from the liquid

$$\left(T_{gas} = T_o + \int_o^x \frac{\rho I^2 / A \, dx}{C_p \dot{m}} \right) .$$

Fig. 5. Schematic drawing of current lead test apparatus. At high flow rates the vacuum-insulated finned-tube heat exchangers operate well below ambient temperature, significantly reducing the resistivity of the current leads.

Fig. 6. First lead configuration test results; voltage vs. current for various mass flow rates.

Fig. 7. First lead configuration test results. Instability boundary was computed assuming constant insulation thermal conductivity for each lead segment and the Nusselt equation (text p. 7) for turbulent flow.

Fig. 8. Second lead configuration results. Resistive heating for one lead.

	I(amps)	$\dot{m}$ (gm/sec)
◇	60.	0.75
●	80.	0.75
○	100.	0.72
△	110.	0.75
□	120.	0.70
▽	125.	0.72
■	131.	0.68
◆	all tests	

Fig. 9. Second lead configuration zero current tests. (four leads)

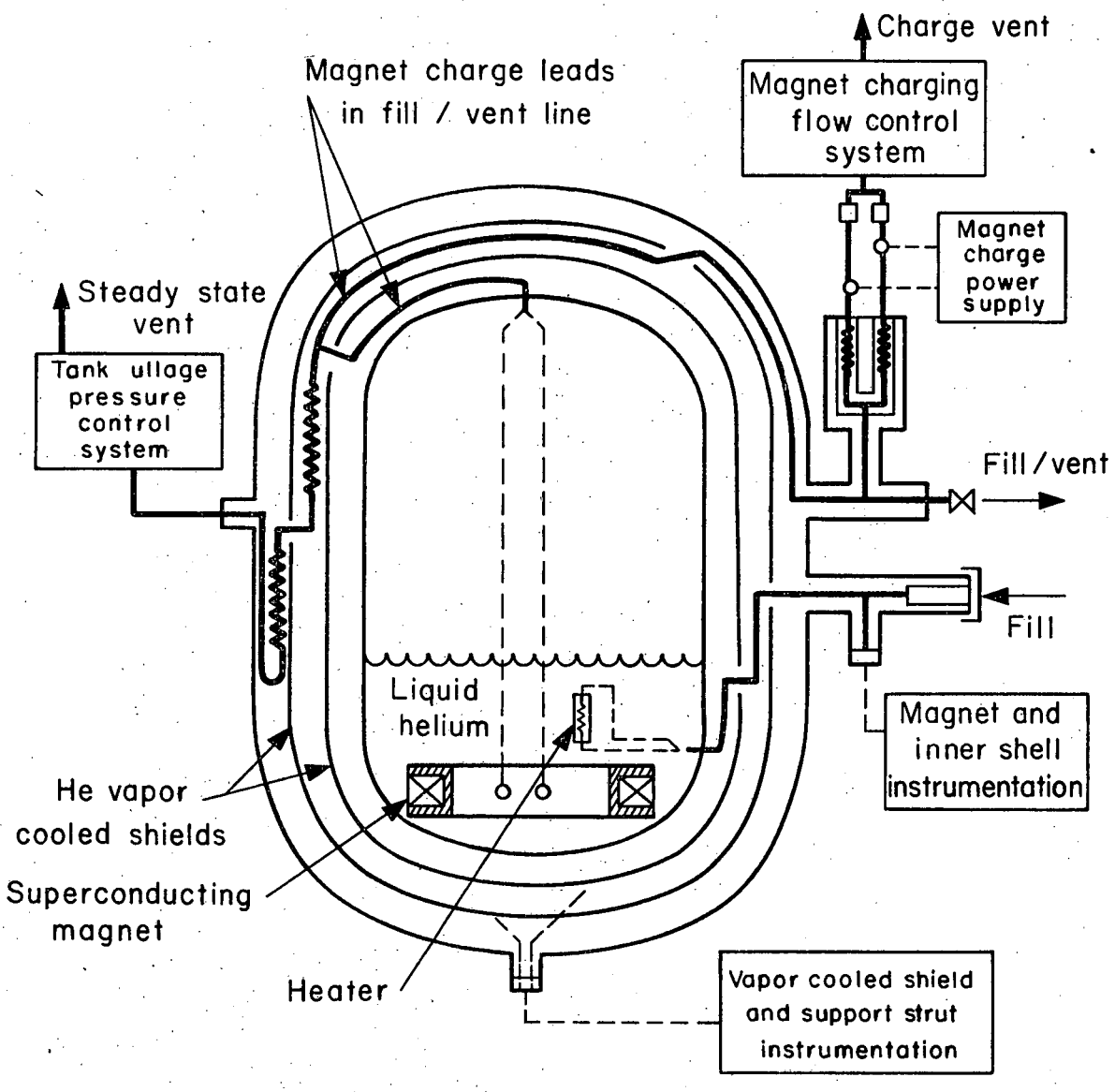

Fig. 1

XBL 743-2695

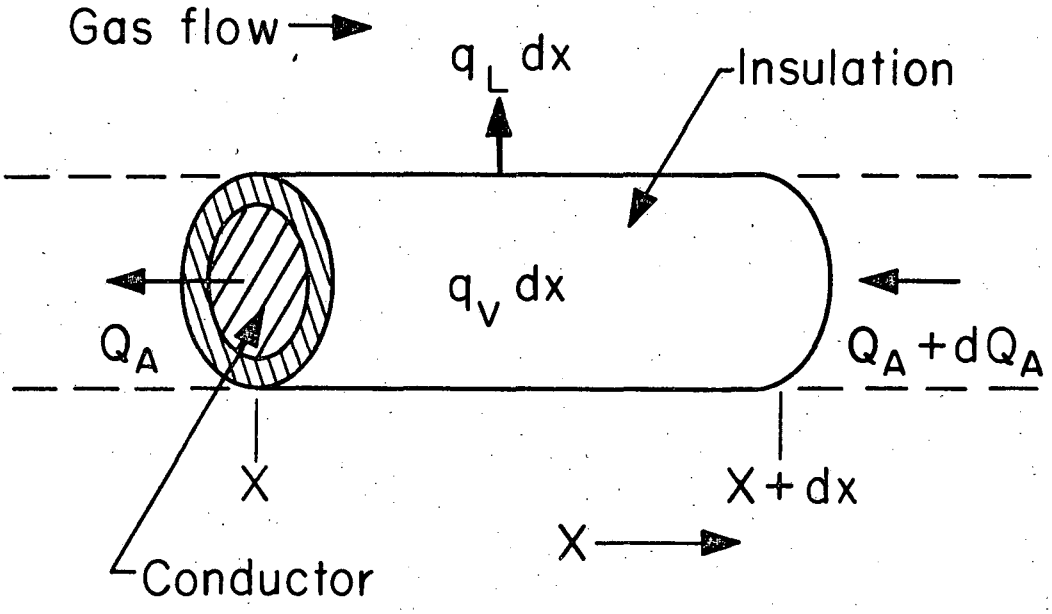

Fig. 2 XBL 743-2720

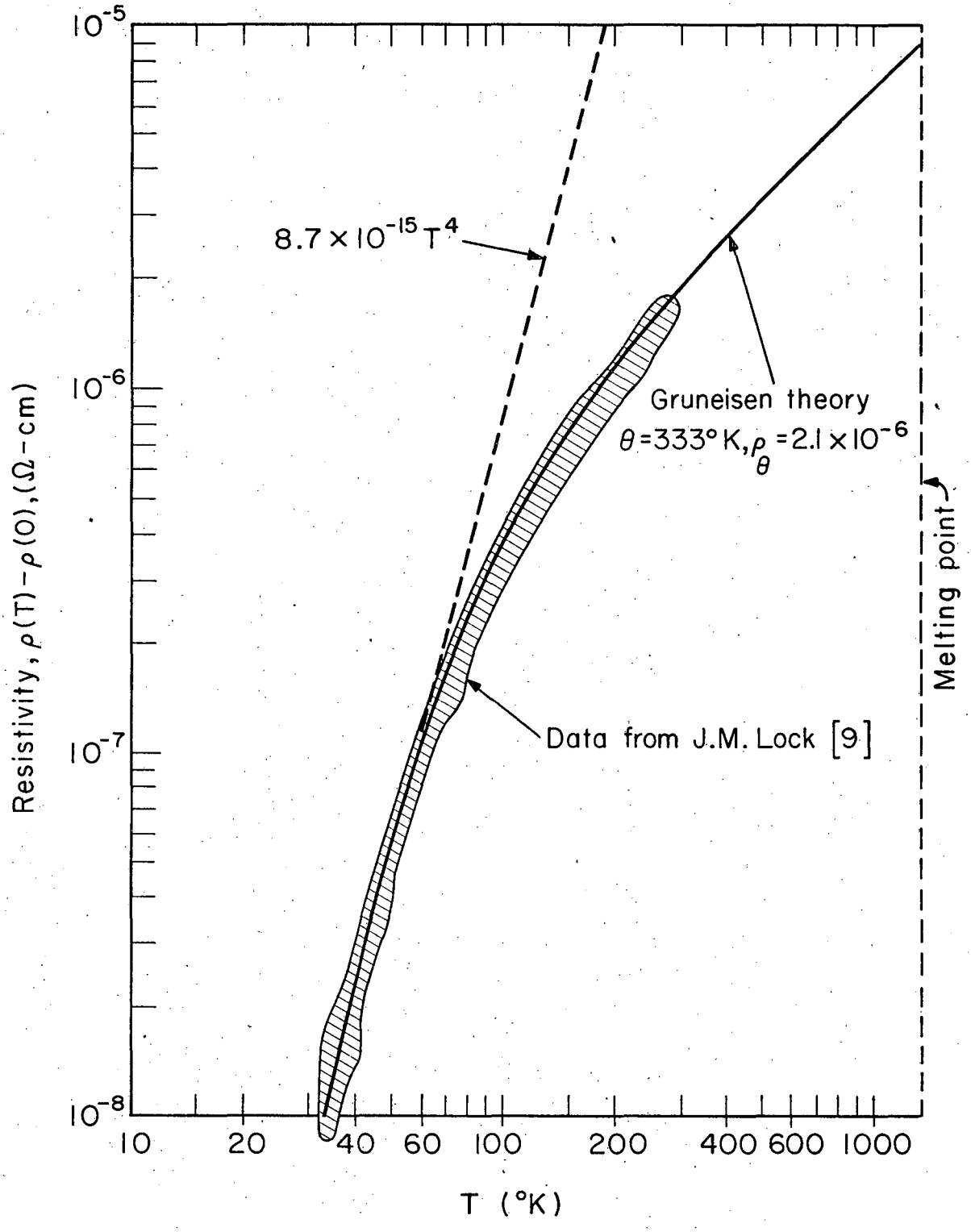

Fig. 3

XBL 743-2719

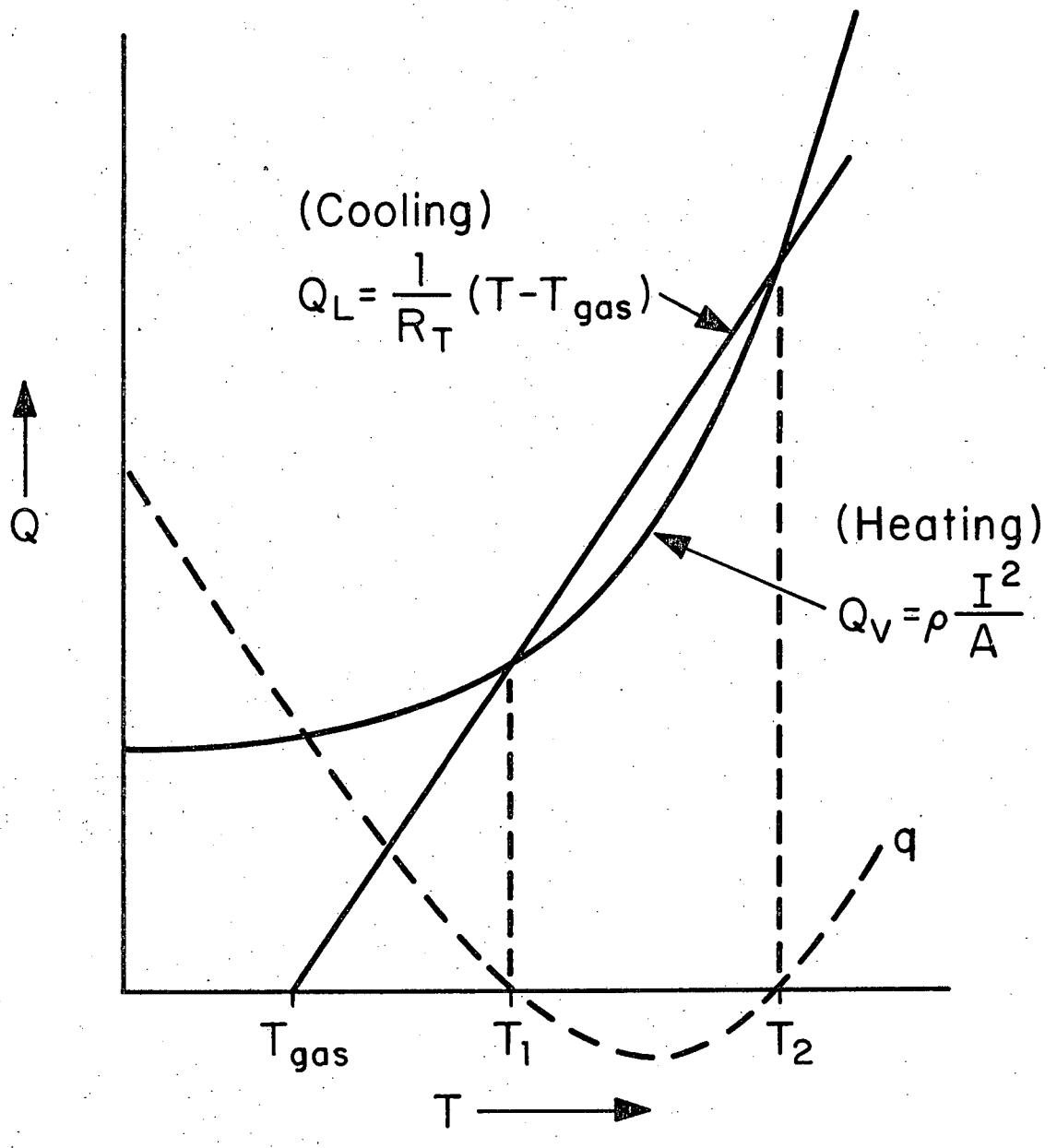

Fig. 4 XBL 743-2721

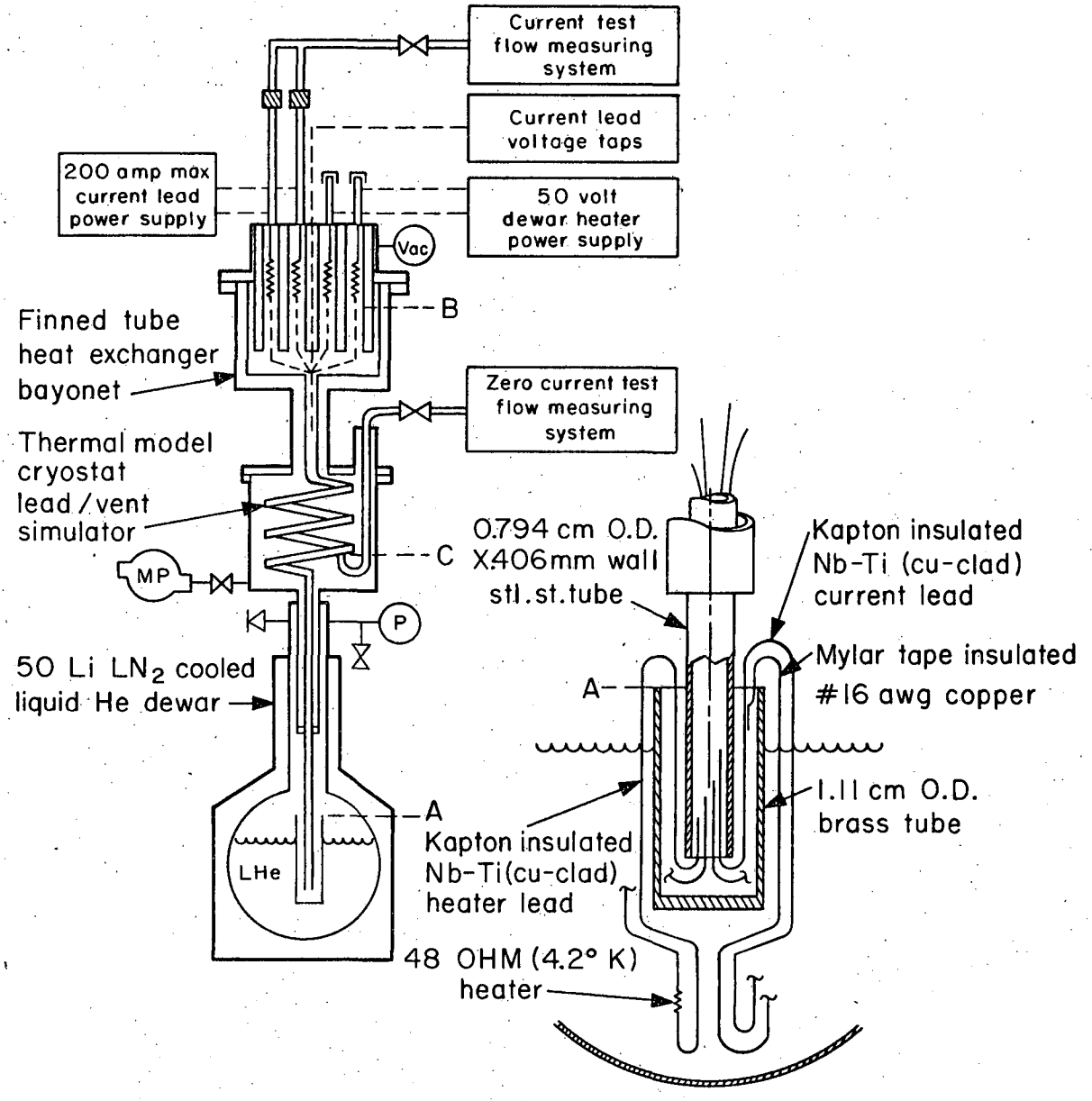

Fig. 5

XBL 743-2694

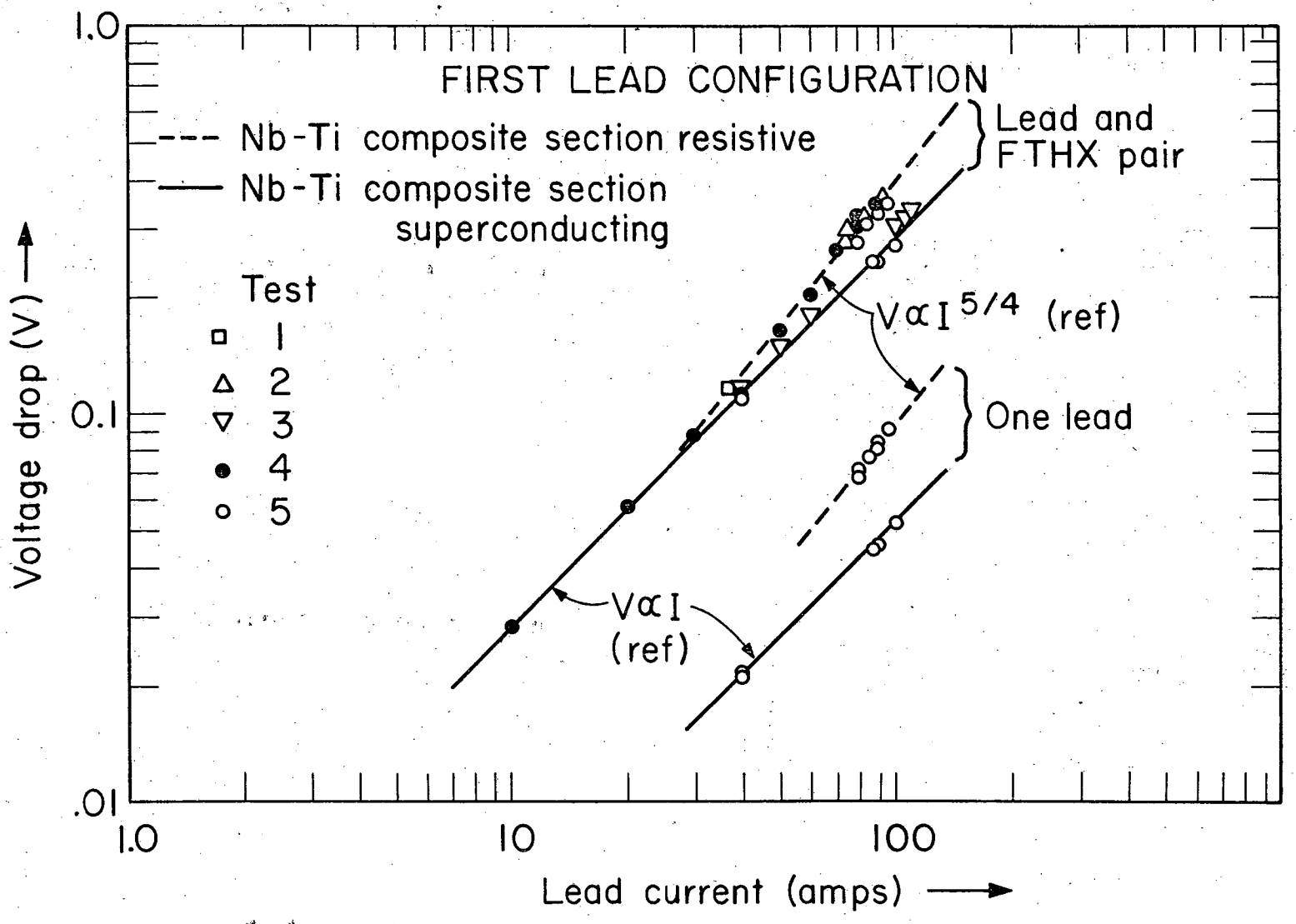

Fig. 6

XBL 744-2776

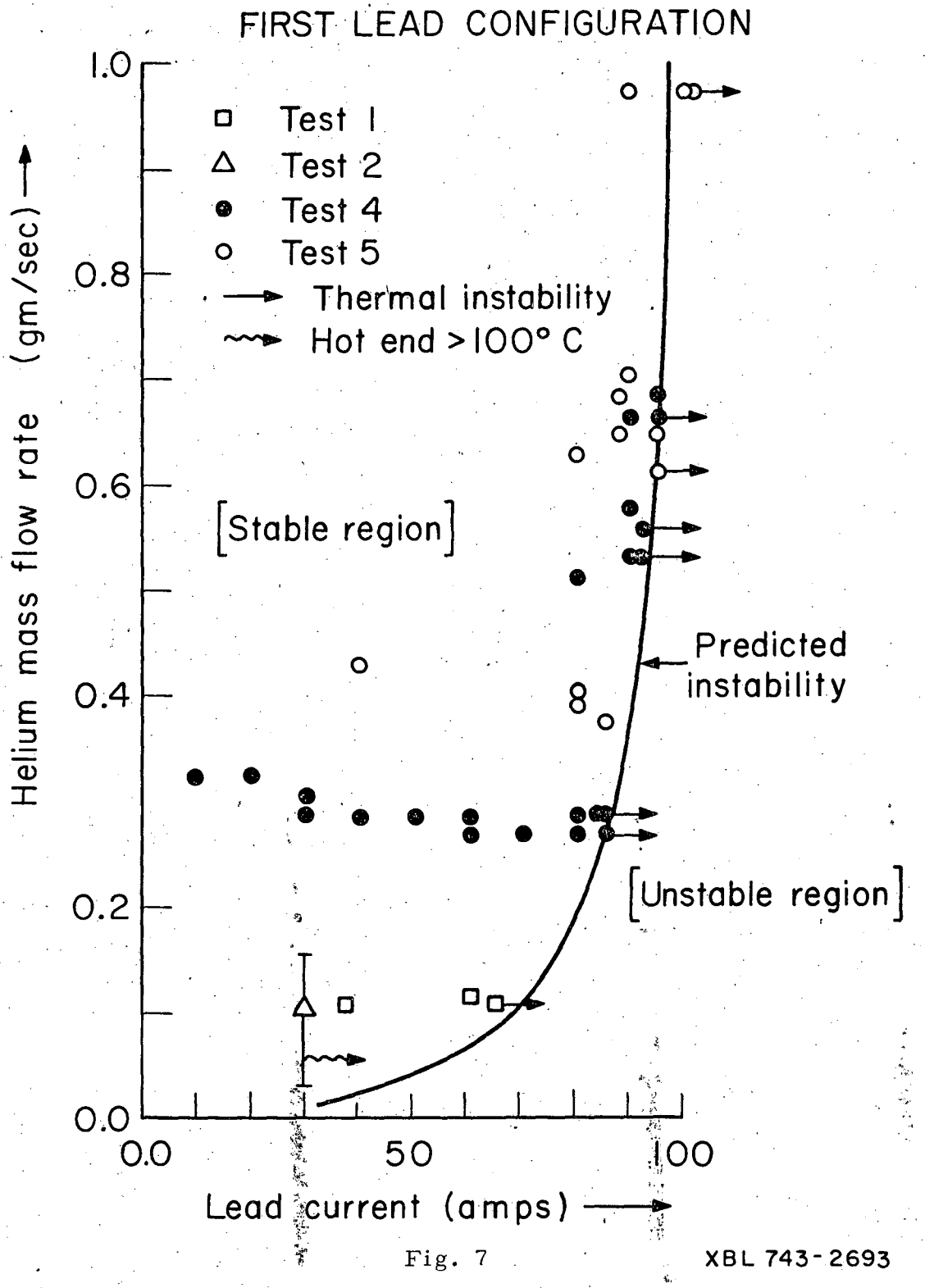

Fig. 7

XBL 743-2693

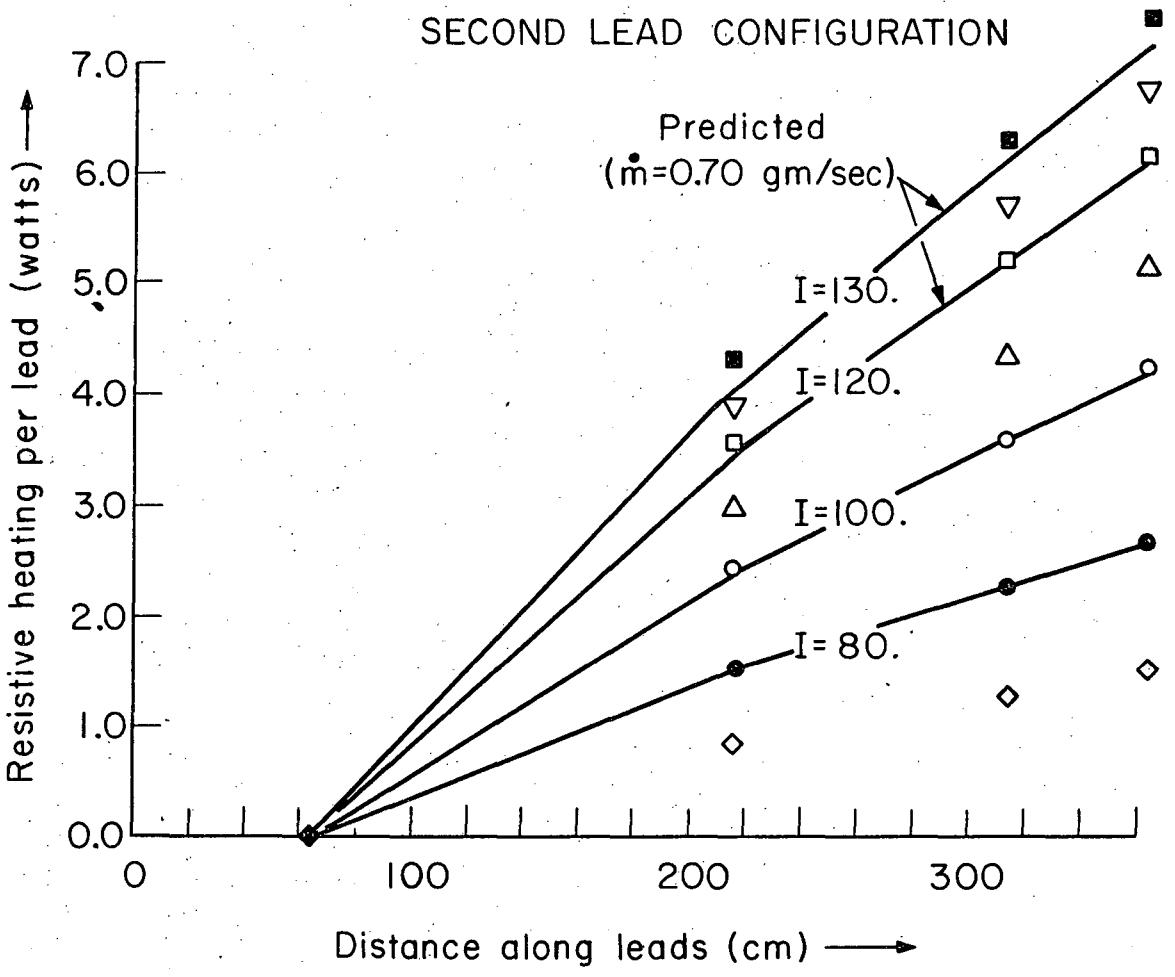

Fig. 8

XBL 743-2691

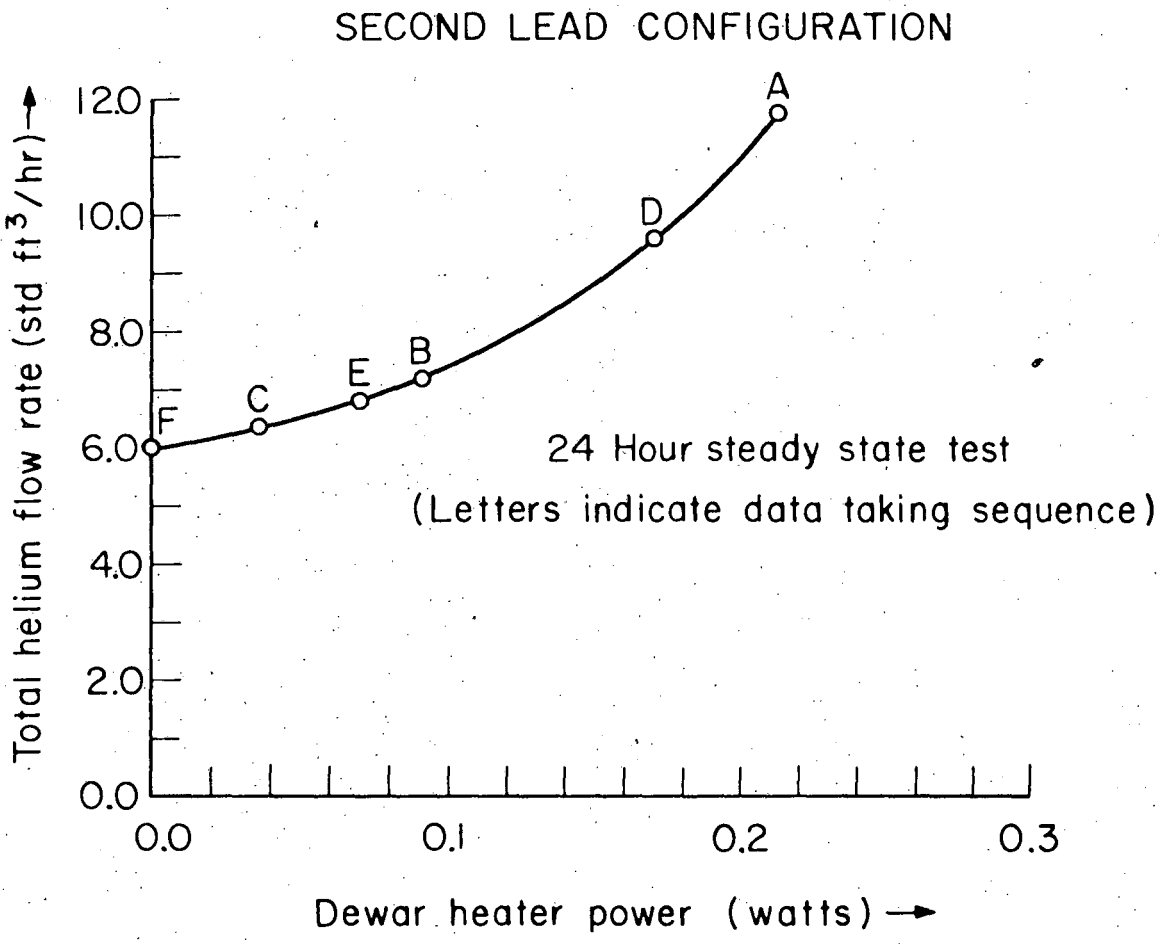
SECOND LEAD CONFIGURATION
Total helium flow rate (std ft³/hr)
12.0
10.0
8.0
6.0
4.0
2.0
0.0
0.0
0.1
0.2
0.3
A
D
B
E
C
F
24 Hour steady state test
(Letters indicate data taking sequence)
Dewar heater power (watts)
XBL 743-2692

Fig. 9

TECHNICAL INFORMATION DIVISION
LAWRENCE BERKELEY LABORATORY
UNIVERSITY OF CALIFORNIA
BERKELEY, CALIFORNIA 94720